Electronic Supplementary Material (ESI) for Physical Chemistry Chemical Physics.

Supplementary Information

Promoting Effect of Tetravalent Cerium on the Oxygen Evolution Activity of Copper Oxide Catalysts

Zhu Chen[1], Coleman X. Kronawitter[2], Xiaofang Yang[1], Yao-wen Yeh[3], Nan Yao[4], Bruce Koel[1]*

[1]Department of Chemical and Biological Engineering, Princeton University, Princeton, NJ 08540

[2]Department of Chemical Engineering, University of California, Davis, Davis, CA 95616

[3]Department of Electrical Engineering, Princeton University, Princeton, NJ 08540

[4]Princeton Institute for the Science and Technology of Materials, Princeton University, Princeton, NJ 08540

Table of Contents

Determination of the elemental composition of pure and Ce-modified CuO_x by EDX

Elemental compositions of pure and Ce-modified samples were obtained using EDX and summarized in Table S1. The Ce concentration increased with increasing Ce mole ratio of the deposition solution as expected.

Table S1 Elemental composition of pure and Ce-modified CuO_x samples by EDX (10 keV electron energy)

Sample	C (at%)	O (at%)	Cu (at%)	Ce (at %)
Cu100Ce0	15.0	50.1	34.9	0
Cu90Ce10	13.0	57.6	28.7	0.7
Cu80Ce20	14.5	58.7	23.9	2.9
Cu70Ce30	16.3	60.2	20.2	3.3
Cu60Ce40	13.1	60.2	21.9	4.8
Cu50Ce50	14.6	60.5	18.2	6.7
Cu40Ce60	16.8	61.5	14.1	7.6

Elemental mapping of pure and Ce-modified CuO_x by EDX

Elemental mapping was also carried out using EDX, which illustrates uniform distribution of Ce and Cu in all samples on the micrometer scale based on the lateral resolution of EDX, which is on the order of micrometer. As a result, EDX mapping cannot distinguish the sub-micron domains of segregated CeO_2 in CuO_x (Ce > 6.9 at%), despite direct observation of such segregation in Raman spectroscopy.

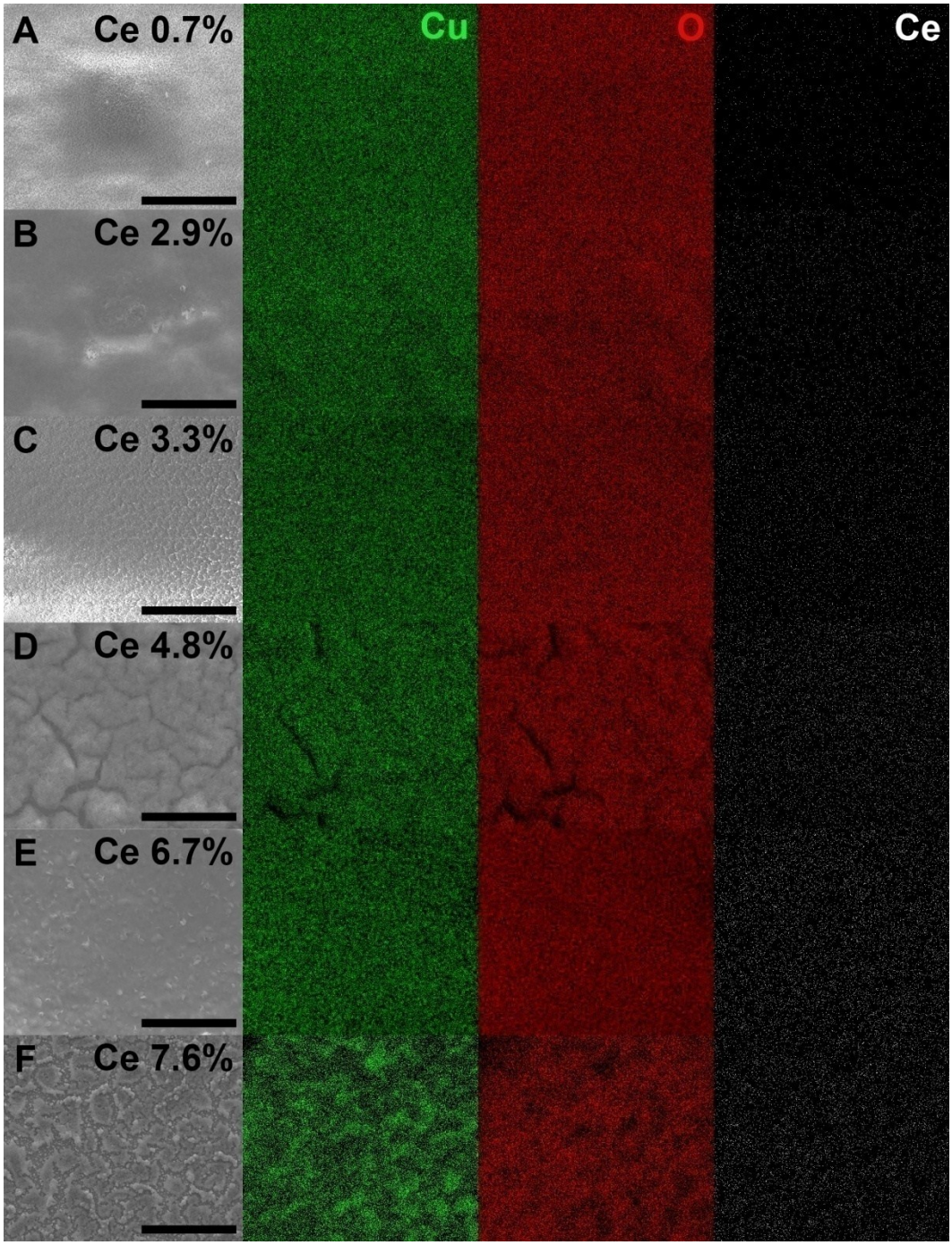

Figure S1 Elemental mapping of pure and Ce-modified samples. The scale bars represent 10 µm.

Determination of the elemental composition of pure and Ce-modified CuO_x by XPS

Compared to the Ce concentration obtained by EDX, the greater Ce content by XPS indicates enrichment of Ce at the surface. The assumption is that Ce is uniformly distributed over the sampling depth of Ce 3d photoelectron (B.E. 917 eV).

Table S2 Elemental composition of pure and Ce-modified CuO_x samples by XPS (150 W, Al kα)

Sample	C (at%)	O (at%)	Cu (at%)	Ce (at%)
Cu100Ce0	16.8	57.7	25.5	0
Cu90Ce10	22.4	48.7	27.0	1.9
Cu80Ce20	26.9	55.8	13.5	3.8
Cu70Ce30	31.4	53.1	10.5	5.0
Cu60Ce40	23.2	57.1	12.8	6.9
Cu50Ce50	29.3	53.2	9.0	8.2
Cu40Ce60	28.6	55.6	5.5	10.3

Characterization and Electrochemical Performance of electrodeposited CeO_2

CeO_2 was electrodeposited onto FTO substrate from a solution containing 0.1 M $Ce(NO_3)_3 \bullet 6H_2O$ at -2.5V. The as-deposited CeO_2 film was dried overnight at 100 °C overnight in a vacuum oven before it was characterized by SEM, Raman and XRD (not shown). OER performance was evaluated using the same method outlined in the experimental section. Based on the SEM images, a dense CeO_2 film was on FTO substrate and showed no preferred morphology. Raman spectrum confirmed the as-deposited film is CeO_2.[7]The OER performance of CeO_2 film is much lower compared to the 6.9 at% Ce-modified CuO_x.

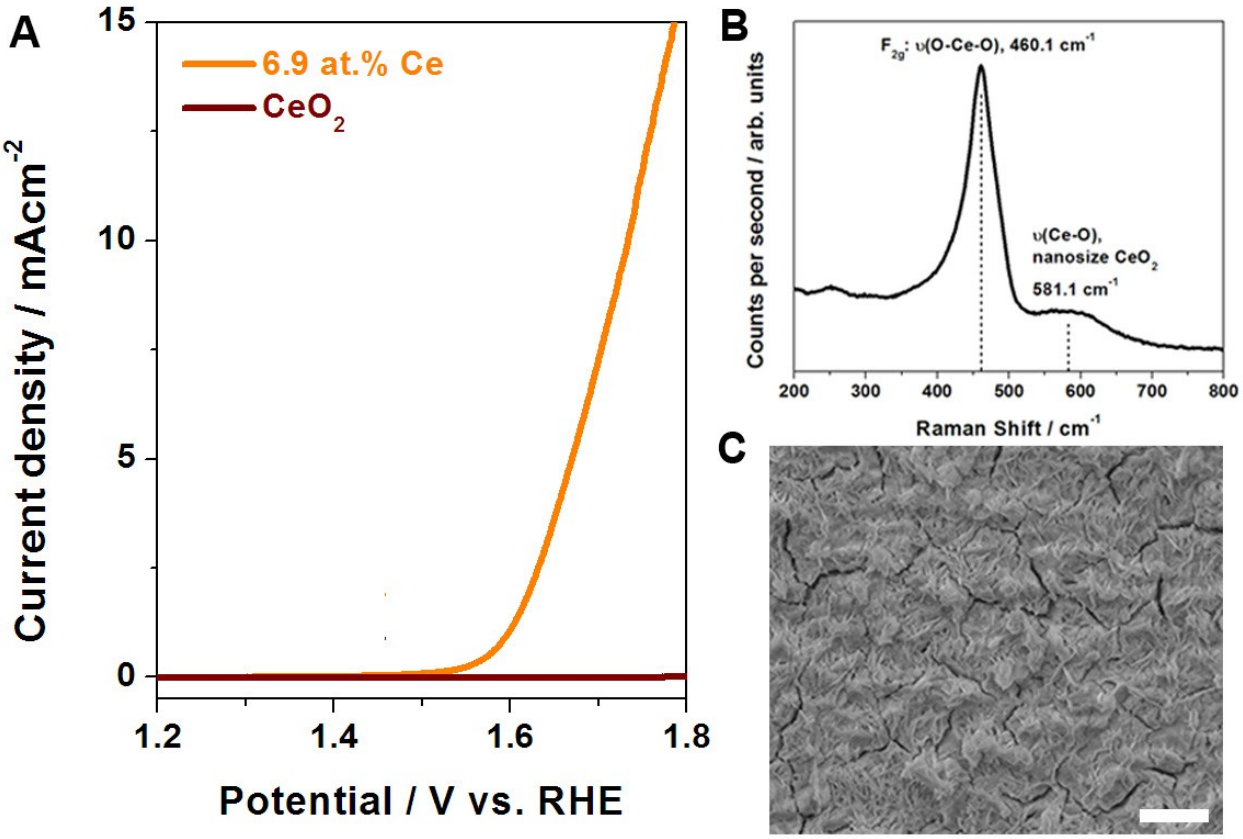

Figure S2 OER performance (A), Raman spectroscopy (B), and SEM image (C) of electrodeposited CeO2 film. The scale bar in (C) represents 5µm.

Tafel analysis of pure and Ce-modified CuO_x samples

Tafel analysis for all samples in the low current density region was carried out. The Tafel slope decreased with increasing Ce concentration reaching an minimum value of 74 $mVdec^{-1}$ at 6.9 at% Ce. This Tafel slope value is close to 60 $mVdec^{-1}$, which can be associated with a rate-limiting chemical step following the first electron transfer. The near-continuous decrease in the Tafel slope with Ce incorporation has been observed by Burke et al, and in the case of Fe-modified CoOOH OER catalyst.[8]At greater Ce concentrations, the Tafel slope value increased to 114 $mVdec^{-1}$indicating poor OER kinetics.

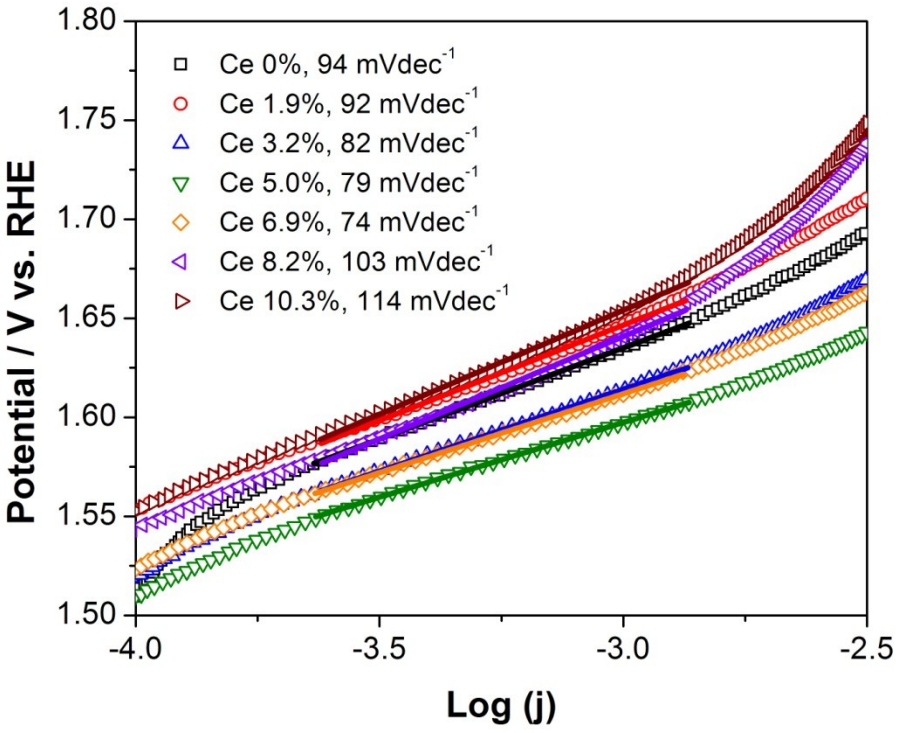

Figure S3 Tafel analysis of pure and Ce-modified CuO_x samples

Double layer capacitance of pure and Ce-modified CuO_x samples

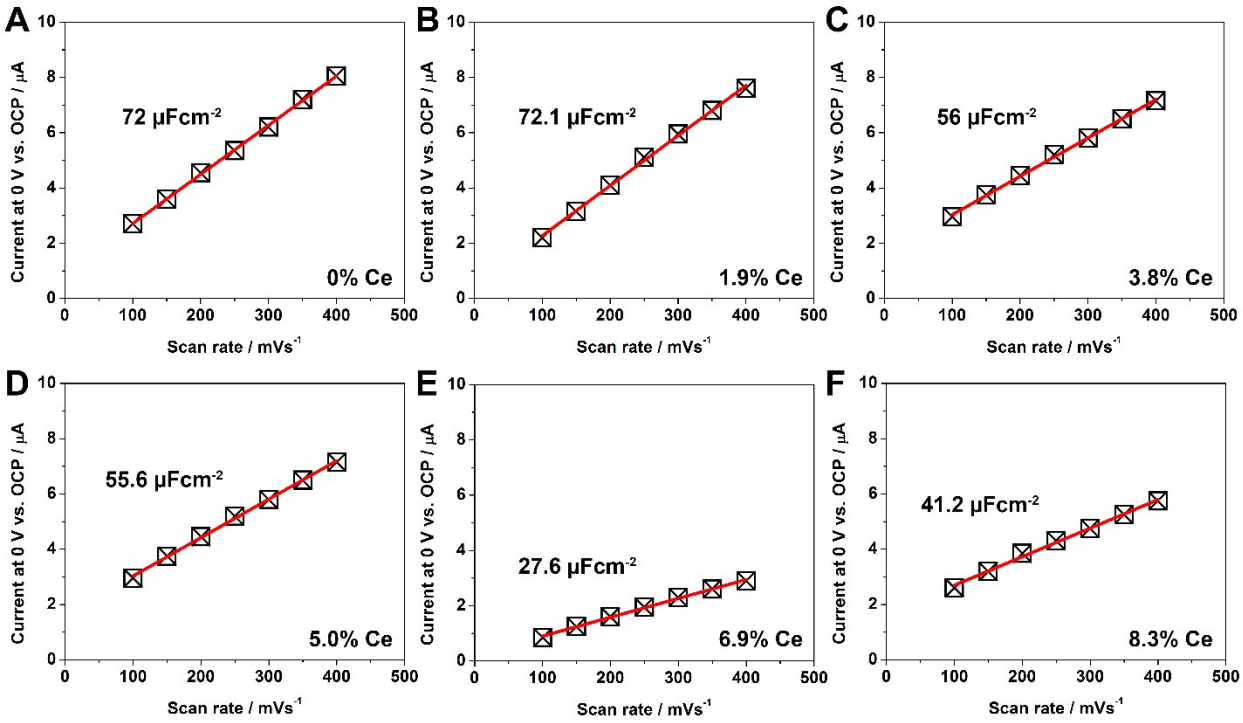

Figure S4 Plots of current density at 0 V vs. the open circuit potential as a function of scan rate. The slope of a linear fit was used to determine the specific capacitance of each catalyst film, for which all had a geometric area of 0.25 cm^{-2}.

"One method for determining the electrochemical active surface area is to measure the double-layer capacitance of the electrode. Cyclic voltammetry experiments were used to measure the capacitive currents of each catalyst at different potential scan rates. The slope of a linear fit to the data in capacitive current vs. scan rate plots was used to determine the capacitance of the catalyst film, which was between 6.9 and 18.1 μF for all samples. Specific capacitance, normalized by the geometric electrode area (0.25 cm^{-2}) was 27.6 to 72.1 μFcm^{-2}. A comparison of the specific capacitance of catalysts with their respective OER activity (Fig. 3) showed no correlation between these two properties. As a result, differences in the surface areas of the films is not a major contributing factor to the OER activity trend reported herein."

Deconvolution of the Ce 3d XPS spectra

The Ce 3d peaks corresponding to Ce^{4+} are the U''' (916.7 eV) and V''' (898.3 eV), which result from the Ce($3d^9$ $4f^0$) O($2p^6$) final states.[1, 2] The other four peaks that are associated with Ce^{4+} [U'' (907.5 eV), V'' (888.7 eV), U (900.7 eV) and V (882.5 eV)] can be attributed to the mixing of of Ce($3d^9 4f^2$)O($2p^4$) and Ce ($3d^9$ $4f^1$)O($2p^5$) final states.[1, 2] The contribution Ce^{3+} to the Ce 3d spectrum are labeled U' (903.2 eV), V'(884.9 eV), U^0 (889.3 eV) and V^0 (881.6 eV) which can be attributed to the mixing of Ce($3d^9$ $4f^1$) O($2p^6$) and Ce($3d^9$ $4f^2$) O($2p^5$) final states.

Table S3 Fitting parameters used for the decomposition of Ce 3d XPS spectra

Components	Cu90/Ce10 (1.9 at% Ce)		Cu80/Ce20 (3.8 at% Ce)		Cu70/Ce30 (5.0 at% Ce)	
	Peak (eV)	FWHM (eV)	Peak (eV)	Peak (eV)	FWHM (eV)	Peak (eV)
Ce^{4+}	916.4	2.3	916.4	2.3	916.5	2.3
	906.2	4.5	906.8	4.6	906.9	4.8
	900.7	2	900.8	2.2	900.8	2.2
	897.8	2.3	898.0	2.3	898.1	2.3
	888.0	4.5	888.4	4.6	888.2	4.8
	882.4	2	882.5	2	882.5	2.2
Ce^{3+}	903.1	4	903.1	3.6	902.8	3.7
	899.0	2.6	899.4	3	899.1	2.4
	884.9	4	885.0	3.6	884.6	3.7
	881.3	2.6	881.5	3	881.4	2.4
Components	Cu60/Ce40 (6.9 at% Ce)		Cu50/Ce50 (8.2 at% Ce)		Cu40/Ce60 (10.3 at% Ce)	
	Peak (eV)	FWHM (eV)	Peak (eV)	FWHM (eV)	Peak (eV)	FWHM (eV)
Ce^{4+}	916.5	2.2	916.4	2.1	916.5	2.1
	907.2	4.5	907.3	4.5	907.2	4.5
	900.7	2.2	900.7	2.0	900.6	2
	898.1	2.2	898.0	2.1	898.2	2.1
	888.2	4.5	888.2	4.5	888.4	4.5
	882.5	2.2	882.4	2.0	882.3	2
Ce^{3+}	902.7	3.7	902.7	3.5	902.6	3
	898.2	2.4	898.4	2.2	898.2	2.4
	884.7	3.7	884.5	3.5	884.3	3
	881.6	2.4	881.7	2.2	881.4	2.4

Calculation of Ce^{3+} and Ce^{4+} composition from Ce 3d XPS spectra

For a quantitative estimation of the Ce^{3+}/Ce^{4+}in Ce-modified CuO_x, the ratio of Ce^{3+}/Ce^{4+}in the total Ce content was calculated from the total integrated areas of the Gaussian fitting peaks for the Ce^{3+}(U^0, U', V^0, V') or Ce^{4+}(U, U'', U''', V, V'' and V''')using the following equations,[3, 4]

$$[Ce^{3+}] = \frac{U^0 + U' + V^0 + V'}{(U + U'' + U''' + V + V'' + V''') + (U^0 + U' + V^0 + V')}$$

$$[Ce^{4+}] = \frac{U + U'' + U''' + V + V'' + V'''}{(U + U'' + U''' + V + V'' + V''') + (U^0 + U' + V^0 + V')}$$

Table S4 Concentration of Ce^{3+} and Ce^{4+} for pure and Ce-modified CuO_x samples determined by XPS

Sample	Ce conc.	Ce^{3+} (%)	Ce^{4+} (%)	Ce^{3+}(at%)	Ce^{4+} (at%)
Cu100Ce0	0	0	0	0	0
Cu90Ce10	1.9	70.6	29.4	1.3	0.6
Cu80Ce20	3.8	43.7	56.3	1.6	2.2
Cu70Ce30	5.0	32.0	68.0	1.6	3.4
Cu60Ce40	6.9	25.3	74.7	1.7	5.2
Cu50Ce50	8.2	25.6	74.4	2.1	6.1
Cu40Ce60	10.3	23.7	76.3	2.4	7.9

Calculation of Cu^{1+} and Cu^{2+} composition from Cu $2p_{3/2}$ XPS spectra

For a quantitative estimation of the different Cu species were carried out using the same procedure adopted for Ce^{3+}/Ce^{4+} as outlined in the previous section. The Cu 2p3/2 XPS spectrum also contains contributions from Cu satellites which was also included in the calculation, as shown in the example below. Additionally, since both CuO and $Cu(OH)_2$ contribute to the satellite and the relative contribution to the satellite feature cannot be accurately determined, we only report the Cu^{2+} and Cu^{1+} concentrations.

$$[Cu^{2+}] = \frac{\left[Cu_{O}^{2+}\right] + \left[Cu_{OH}^{2+}\right] + satellites}{\left[Cu^{1+}\right] + \left[Cu_{O}^{2+}\right] + [Cu_{OH}^{2+}] + satellites}$$

Table S5 Distribution of Cu species for pure and Ce-modified CuO_x samples determined by XPS.

Sample	Cu conc.	Cu^{1+} (%)	Cu^{2+}-O (%)	Cu^{2+}-OH (%)	Cu^{1+} (at%)	Cu^{2+} (at%)
Cu100Ce0	25.5	31.8	25.1	12.2	8.1	17.4
Cu90Ce10	27.0	16.2	16.1	32.3	3.7	19.3
Cu80Ce20	13.5	17.6	15.9	34.0	2.4	11.1
Cu70Ce30	10.5	12.7	18.1	36.2	1.6	11.2
Cu60Ce40	12.8	17.2	30.1	21.0	1.8	8.7
Cu50Ce50	9.0	17.3	29.4	23.8	1.5	7.5
Cu40Ce60	5.5	12.5	36.6	20.9	0.7	4.8

Determination of Cu oxidation state based on Cu LMM Auger spectrum

X-ray excited Auger spectra were used to distinguish Cu metal Cu_2O by the Cu LMM spectra, a distinction that is more difficult from the Cu 2p spectra alone. The kinetic energy of the Cu LMM for Cu metal film is at 918.5 eV, (568.1 eV BE),which does not match with the peak position observed for pure and Ce-modified CuO_x.[5, 6]

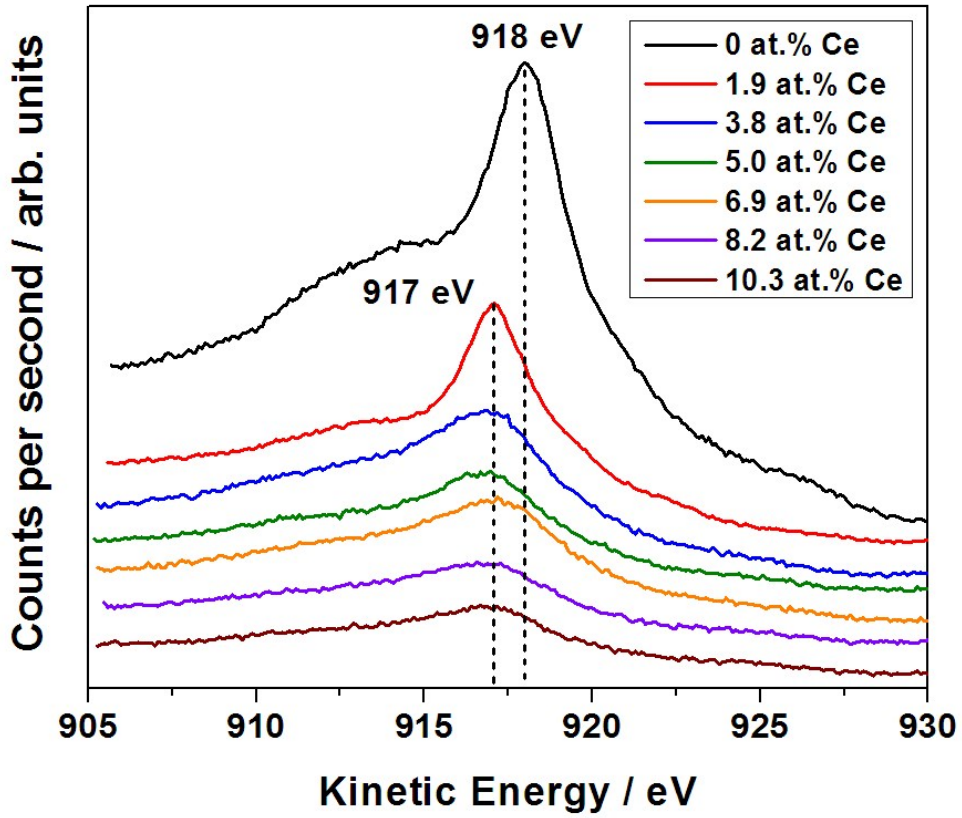

Figure S5 X-ray excited Auger spectra of Cu LMM.

Analysis of surface O species from O 1s XPS spectra

For a quantitative estimation of the different surface O species were carried out using the same procedure adopted for Ce^{3+}/Ce^{4+} as outlined in the previous section.

$$[CuO/Ce^{4+}-O] = \frac{[CuO/Ce^{4+}-O]}{[CuO/Ce^{4+}-O] + [Cu_2O/Ce^{3+}-O] + [OH-CO^{2-}_3] + [H_2O]}$$

Table S6 Distribution of O species for pure and Ce-modified CuO_x samples determined by XPS.

Sample	O conc.	CuO/ Ce^{4+}-O (%)	Cu_2O/ Ce^{3+}-O (%)	OH/CO_3^{2-} (%)	CuO/ Ce^{4+}-O (at%)	Cu_2O/ Ce^{3+}-O (at%)	OH/CO_3^{2-} (at%)
Cu100Ce0	57.7	28.7	22.4	35.7	16.7	13.1	10.4
Cu90Ce10	48.7	18.1	18.4	50.0	8.8	9.0	9.0
Cu80Ce20	55.8	16.7	19.8	49.2	9.3	11.0	8.2
Cu70Ce30	53.1	20.4	17.1	51.0	10.8	9.1	10.4
Cu60Ce40	57.1	33.0	15.1	38.7	18.8	8.6	12.8
Cu50Ce50	53.2	35.2	17.9	37.1	18.7	9.5	13.0
Cu40Ce60	55.6	43.1	13.9	33.3	24.0	7.7	14.4

OER stability, Raman spectroscopy and XPS of pure and Ce-modified CuO_x samples after stability testing.

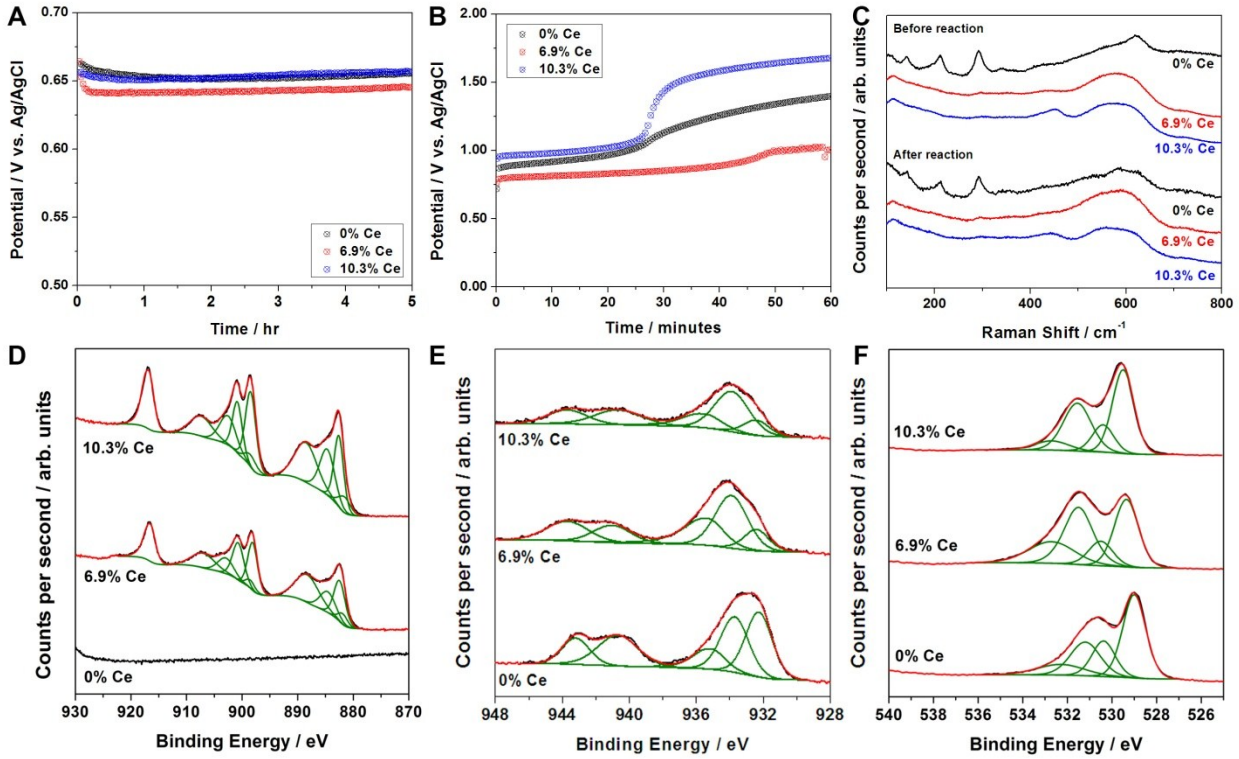

Figure S6 OER stability at 1 $mAcm^{-2}$ (A) and 5 $mAcm^{-2}$ (B), Raman spectroscopy (C) and XPS (D-F) after 1 $mAcm^{-2}$ and 5 $mAcm^{-2}$ stability testing.

Catalyst morphology after stability testing

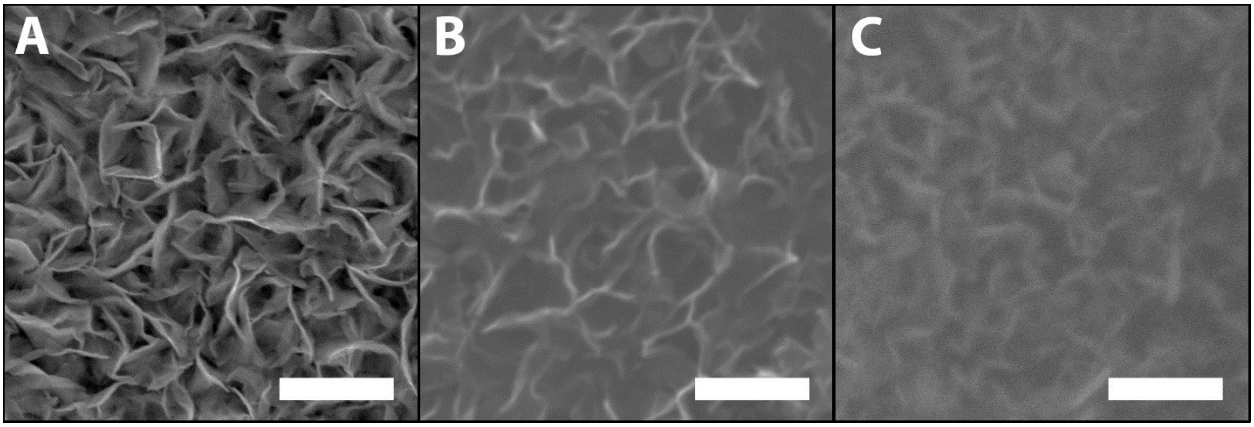

Figure S7 SEM images of A) pure, B) 6.9% Ce and C) 10.3% Ce-containing catalyst after durability testing. These catalysts exhibit similar morphologies compared with those observed prior to OER analysis. No obvious increased in the degree of porosity was observed through qualitative assessment of the SEM images.

References

1. E. Beche, P. Charvin, D. Perarnau, S. Abanades and G. Flamant, *Surf. Interface Anal.*, 2008, **40**, 264-267.
2. P. Patsalas, S. Logothetidis, L. Sygellou and S. Kennou, *Phys. Rev. B*, 2003, **68**, 035104.
3. F. Zhang, P. Wang, J. Koberstein, S. Khalid and S. W. Chan, *Surf. Sci.*, 2004, **563**, 74-82.
4. S. Deshpande, S. Patil, S. V. N. T. Kuchibhatla and S. Seal, *Appl. Phys. Lett.*, 2005, **87**, 133113.
5. S. Poulston, P. M. Parlett, P. Stone and M. Bowker, *Surf. Interface Anal.*, 1996, **24**, 811-820.
6. J. P. Espinos, J. Morales, A. Barranco, A. Caballero, J. P. Holgado and A. R. Gonzalez-Elipe, *J. Phys. Chem. B*, 2002, **106**, 6921-6929.
7. Z. L. Wu, M. J. Li, J. Howe, H. M. Meyer and S. H. Overbury, *Langmuir*, 2010, **26**, 16595-16606.
8. M. S. Burke, M. G. Kast, L. Trotochaud, A. M. Smith and S. W. Boettcher, *J. Am. Chem. Soc.*, 2015, **137**, 3638-3648.